Title: Computational Discovery of Extremal Microstructure Families

Authors: Desai Chen[1*], Mélina Skouras[1], Bo Zhu[1], Wojciech Matusik[1]

Affiliations:

[1]MIT CSAIL.

*Correspondence to: desaic@csail.mit.edu.

Abstract: Modern fabrication techniques such as additive manufacturing can be used to create materials with complex custom internal structures. These engineered materials exhibit a much broader range of bulk properties than their base materials, and are typically referred to as metamaterials or microstructures. While metamaterials with extraordinary properties have many applications, designing them is very difficult and is generally done by hand. We propose a computational approach to discover families of microstructures with extremal macroscale properties automatically. Using efficient simulation and sampling techniques, we compute the space of mechanical properties covered by physically realizable microstructures. Our system then clusters microstructures with common topologies into families. Parameterized templates are extracted from families to generate new microstructure designs. We demonstrate these capabilities on the computational design of mechanical metamaterials and present five auxetic microstructure families discovered by our algorithm. Our study opens the way for completely automated discovery of extremal microstructures across multiple domains of physics, including applications reliant on thermal, electrical and magnetic properties.

One Sentence Summary: We propose the first fully computational method for discovering microstructure families with extremal physical properties.

Main Text: Microstructures can exhibit remarkable physical properties that extend beyond the properties of their constituent materials. Many microstructure types have been developed to demonstrate applications in mechanics (*1-6*), acoustics (*7,8*), and electromagnetics (9-11). These microstructures are typically designed by domain experts using time and labor intensive manual processes. These designs are often programmable in the sense that they have a small number of parameters to generate a family of geometries. A given microstructure family can be tested by performing simulations or experimental measurements on a set of samples drawn from it. The mapping between parameters and physical properties discovered in this testing process helps uncover the underlying design principles that drive these correspondences. In practical applications, mapping the parameter space also allows for the selection of a family member that has a desired tradeoff of physical properties, allowing it to achieve some desired performance objective (*12*). Unfortunately, it is rare for manually designed microstructure families to reach extremal properties. This is because the space of possible microstructure designs is combinatorial and therefore impossible to explore exhaustively. One common approach to bypass this design challenge is to use computational methods, such as topology optimization (*13-15*), with a computer simulation in their inner loop to find a microstructure with a desired tradeoff of physical properties. Unfortunately, constructing parametric models from these optimized structures has heretofore required further expertise and manual design effort (*16*). In contrast to previous work, we present the first computational method to automatically explore the space of microstructure designs and discover parametric families optimized for competing properties.

While our methodology is not limited to specific physical properties, this study applied our method to design of mechanical microstructures. Specifically, we set our algorithm to search for a particularly interesting type of mechanical microstructures: auxetic materials, which have a negative Poisson's ratio. These materials have the unusual property of becoming laterally thinner under axial compression. 2D auxetic structures are well understood due to their relatively simple geometry such as reentrant structures (*17, 13*), chiral structures (*18, 19*) and rotating mechanisms (*20-22*). Generalizing existing 2D structures to 3D is challenging since a naive arrangement of 2D mechanisms often results in orthotropic or other anisotropic structures with low shear resistance. Such structures will prefer shearing deformation when the load is not aligned well with the auxetic direction. Additionally, since Poisson's ratio for orthotropic structures is unbounded, orthotropic auxetic structures are much easier to find than isotropic ones (*23*). Lakes (*17*) fabricated and tested the first isotropic 3D auxetic structure. However, designing manufacturable 3D auxetic structures remains a challenging task due to its complexity. Only a handful of 3D design patterns have been fabricated and measured (*23, 24*). This case study led to the discovery of five families with negative Poisson's ratio and tunable shear resistance.

Our discovery pipeline has four steps (figure 1). The first step estimates the material property gamut, which is the range of material properties achievable by the microstructures. Here a microstructure is defined on a 3D regular grid composed of hexahedral voxels. The design space includes all possible material assignments to the voxels. Since exhaustively simulating all possible microstructures is impractical, this step computes a set of sample microstructures. The sampling algorithm alternates between topology optimization and stochastic discrete search to progressively expand the gamut (*25*). The topology optimization stage pushes structures past the explored gamut boundary along gradient directions. The stochastic stage introduces discrete changes to escape local optima.

In the second step, common geometric traits are identified among microstructures near the gamut boundary. Geometrically similar structures are grouped into families using nonlinear dimensionality reduction (NLDR). Isomap (*26*) is used as the reduction method because it can discover long sequences of related structures while keeping distant points separated. The effectiveness of NLDR depends on the distance metric that measures geometric difference. A smoothed Euclidean norm is chosen for robustness (figure S1). NLDR outputs an embedding of the microstructures in a low-dimensional space where similar structures are closely packed. Microstructures in the embedding space are clustered using a Gaussian mixture model (*27*) where each cluster corresponds to a family. Families with a significant number (>200) of members are extracted for further analysis.

The third step in our process constructs templates for each microstructure family. We observe that most of the extremal structures are composed from beams, plates and blocks. All of these structures can be represented as cuboids with different edge lengths. We therefore chose cuboids as the building blocks for microstructure templates, and note that some structures near the boundary do not fit the cuboid representation (figure. S4). To find a template from a family representative, its topology is computed using a morphological skeleton (*28*). The morphological skeleton is a set of connected edges that largely preserves topological and branching characteristics of the structures. The skeleton is converted into a graph in order to represent a template. A cuboid is placed on each edge of the graph with optimized sizing and orientation to best match the representative structure. More details of the process are available in the supplementary text.

Finally, reduced parameters are computed to allow an intuitive navigation in the material property space. Since the templates from the previous step contain tens of parameters that do not directly correspond to material properties, it is still difficult to understand the key design principles. The reduced parameters allow for direct tuning of each material property. For a given parametric template, its parameters are fitted to all structures of the corresponding family. To avoid outliers, microstructures leading to large fitting errors (>5% voxel difference) are excluded. Principal component regression (PCR) is then performed on the set of fitted template parameters to find principal directions in the template parameters space. Varying the parameters in a direction corresponds to moving on the gamut boundary in a certain direction. A reduced parameter is assigned to each direction to control amount of change along that direction.

The results of this study focus on elastic material properties: Young's modulus, Poisson's ratio and shear modulus. The elastic material property gamut is estimated from 15,000 3D cubic-symmetric microstructures at a voxel resolution of 64^3 (*29*). The voxel resolution is a power of 2 because that is necessary to achieve optimal performance of our multigrid FEM simulation. The specific resolution 64^3 is chosen because it is sufficient for discovering auxetic structures with a wide range of relative shear modulus while 32^3 structures cannot achieve comparable complexity or property ranges. The macroscopic elastic parameter of each microstructure is computed using homogenization theory (*30, 31*) assuming a periodic boundary condition, (i.e. the structure is repeated infinitely). Each microstructure consists of a per-voxel binary material assignment. Due to manufacturing limits on minimum feature size, sensitivity filtering (*32*) is applied in gamut sampling step to avoid structures with overly thin features.

Here we report deeper analysis for auxetic structures from the gamut since families with positive Poisson's ratios are relatively simple (figure S2). Five families with significant number of members (figure. 2B) are discovered using three Isomap embedding dimensions. We confirmed that Isomap associates seemingly distant structures through intermediate structures. For example, structures 5-1 and 5-3 from family 5 have very different beam thicknesses resulting in large geometric distance. However, the embedding reveals that there is a sequence of structures such as 5-2 that make the connection between them.

Parametric templates are constructed for all five families. The initial topology of the templates is extracted from morphological skeletons (figure 3B). While the topologies are visually complex, they are generated by mirroring a small number of beams (highlighted in red) reflected according to cubic symmetry (Table S2). The most complex template 5 contains only 6 control beams. The five families cover similar ranges of Young's modulus and Poisson's ratio. However, they span different ranges of shear modulus. Inspired by classical linear elasticity theory, we compare the shear modulus ratio defined as

$$G' = \frac{2G(1+v)}{E},$$

where G is shear modulus, E is Young's modulus and ν is Poisson's ratio. For traditional isotropic materials, the theoretical ratio is one. A low ratio indicates low resistance to shear deformation. For auxetic materials, lower ratios are much easier to obtain than higher ones. Even with foam structures assumed to be isotropic, experimental data from previous work indicates that the ratio is less than one (*33*).

Template 1 resembles the conceptual sketch by Lakes (*17*) and belongs to the reentrant class of geometry. The difference is that our template has only two beams mirrored by cubic

symmetry while Lakes' sketch contains three (Fig. S6). It is the simplest auxetic template that we identified, as our microstructure database does not contain any single-beam auxetic structure. The shear modulus ratio of this family falls in the range between 0.07 and 0.24, which is the lowest among all five families. Templates 2 and 3 are similar to each other and differ by a diagonal beam in the face center (highlighted in green in template 3). Since their geometric difference is small, they are adjacent in the Isomap embedding space. The central beam is responsible for increasing the shear modulus of the structures. For structures with ν around -0.5, the additional beam increases the maximum shear modulus ratio from 0.34 to 0.90. Templates 4 and 5 also differ by a single beam. Even the most complex template 5 is optimized from a simple cube frame through our continuous optimization step as shown in our supplemental material (video S1). The additional beam in template 5 makes the family stiffer overall. Both families can achieve shear modulus ratio greater 1 for ν<-0.5.

For each family, principal directions of template parameters are extracted using PCR. The templates and reduced parameters are included with the report (*29*). Two significant directions correspond to change in Young's modulus and shear modulus are kept for tuning structures. These directions reveal that for families 2 and 3, the thickness of the slanted column (Fig. 4a highlighted in red) is crucial for Poisson's ratio where the Poisson's ratio increases quickly with increasing beam thickness. For families 4 and 5, the thickness of the rotating triangle (figure 4B) affects the tradeoff between Young's modulus and shear modulus (figure S5).

While our cuboid-based templates are very simple, they are sufficient for replicating the auxetic behavior of the corresponding families. We validated the auxetic properties of the fitted microstructures using simulation. New structures are generated by varying template parameters. 300 new structures are sampled from each family along two PCR coordinate directions. The coverage of the templates in the microstructure gamut (figure 2B) shows that the templates can generate microstructures on the gamut boundary

So far all of our simulations are carried out assuming linear elasticity, which is only accurate for infinitesimal deformations. We also make the common assumption that there is no self-collision. This assumption also imposes a limit on the maximum compressive strain we can apply to our structures before self-collision occurs. Representative structures from Families 4 and 5 have the lowest limit at 7% compressive strain. In practice, non-linear deformations such as bending and rotation are prevalent in our auxetic structures. Such deformations can cause linear elasticity to incorrectly predict significant volume expansion of rotated parts (up to 20% percent in our test cases). Thus, we tested our structures using a nonlinear deformation model to understand their behavior under large deformations. We simulated nonlinear deformation behavior using Neo-Hookean material model (*34*). At maximum allowed strain of 7%, linear elasticity and Neo-Hookean model still has acceptable agreement with an average error of 16% in computed Poisson's ratio. In addition to simulation, we also manufactured three example structures from each family with varying Young's modulus and material ratio. All the structures are printed using a single elastic material (*35*). Our structures demonstrated consistent auxetic behavior (videos S3) even though they are optimized with linear elasticity assumption. Our structures do not rely on structural instability (*36*) for auxetic behavior and shrinks uniformly as load increases. This means that their deformations consistently follow the same pattern for different trials.

Our process automatically discovered two types of auxetic mechanisms: slanted columns and rotating triangles (figure 4). The slanted column mechanism transforms vertical compression

to horizontal motions. The rotating triangles transform vertical compression into a winding deformation that pulls the right end of the mechanism towards the center of the microstructure. Their motions are shown in supplementary video S3. While rotating triangles bear resemblance to existing 2D structures (*37*) known as chiral structures (figure S6D), its extension to 3D cubic structure with large shear modulus has never before been constructed. Additionally, the entire mechanism is discovered entirely automatically without imposing any artificial design restrictions – all microstructures are built from hexahedral voxels. To inspire future applications of these mechanisms, we report the loading behavior of the mechanisms. These auxetic mechanisms are the most active parts in the microstructures. They act like joints that connect the more rigid scaffolding in microstructures. Because of this, they undergo the most deformation and concentrate a large amount of stress. For the rotating triangles, the stress is concentrated on the connections around the triangle. We computed the maximum principal strain in the structure with respect to the vertical compressive loading to provide insights into the strength of the block. At the maximal compressive loading (7%), the maximum principal strain in the structure is 7%. Calculation using a reported Young's modulus of 80MPa yields a von Mises stress of 6.72MPa (figure 4E) while our print material has a reported strength of 8.5MPa. The printed structures are approaching the strength limit under the load. Since the available material is relatively weak even compared to common materials such as ABS plastics and rubber, we believe that structural strength can be improved significantly with future manufacturing materials.

We have shown a computational method that combines discrete sampling, continuous optimization and dimensionality reduction methods for automatic discovery of new microstructure families and mechanisms that would have been challenging to design manually. The discovered structures are suitable for manufacturing as they avoid thin features and distribute deformation over beams instead. They also span a wide range of shear moduli, allowing engineers to balance between different macroscopic properties. While our case study focuses on elastic material properties, the technique may be applied to other physical properties whenever predictive simulation exists. Our computational pipeline paves the way to discovery of structures that balance mechanical, thermal, optical, acoustic and electromagnetic properties. Moreover, it advances the understanding of underlying mechanisms that are key to extremal properties.

References and Notes:

1. G. W. Milton, A. V. Cherkaev, Which elasticity tensors are realizable? *J. Eng. Mater.* **117**, 483-493 (1995). doi: 10.1115/1.2804743

2. M Kadic, T Bückmann, N Stenger, M Thiel, M Wegener, On the practicability of pentamode mechanical metamaterials. *Appl. Phys. Lett.* **100**, 191901 (2012). doi: 10.1063/1.4709436

3. L. R. Meza, S. Das, J. R. Greer, Lightweight, and recoverable three-dimensional ceramic nanolattices, *Science* **345**, 1322-1326 (2014). doi: 10.1126/science.1255908

4. X. Zheng *et al.*, Ultralight, ultrastiff mechanical metamaterials, *Science* **344**, 1373-1377 (2014). doi: 10.1126/science.1252291

5. Q. Wang *et al*., Lightweight Mechanical Metamaterials with Tunable Negative Thermal Expansion. Phys. Rev. Lett. **117**, 175901(2016). doi: 10.1103/PhysRevLett.117.175901

6. X. Li, H. Gao, Mechanical metamaterials: Smaller and stronger. *Nat. Mater.* **15**, 373–374 (2016). doi: 10.1038/nmat4591

7. N. Fang *et al.*, Ultrasonic metamaterials with negative modulus, *Nat. Mater.* **5**, 452-456 (2006). doi: 10.1038/nmat1644

8. J. Li, L. Fok, X. Yin, G. Bartal, X. Zhang, Experimental demonstration of an acoustic magnifying hyperlens, *Nat. Mater.* **8**, 931-934 (2009). doi: 10.1038/nmat2561

9. D. Schurig *et al.*, Metamaterial Electromagnetic Cloak at Microwave Frequencies, *Science* **314**, 977-980 (2006). doi: 10.1126/science.1133628

10. V. M. Shalaev, Optical negative index metamaterials. *Nature Photon.*, **1**, 41–48 (2007). doi: 10.1038/nphoton.2006.49

11. F. Magnus et al., A d.c. magnetic metamaterial. Nat. Mater. 7, 295 (2008). doi:10.1038/nmat2126

12. L. J. Gibson, M. F. Ashby, G. S. Shajer, C. I. Robertson, The mechanics of three-dimensional cellular materials, *Proc. R. Soc. Lond. A* **382**, 25-42 (1982). doi: 10.1098/rspa.1982.0088

13. O. Sigmund, Materials with prescribed constitutive parameters: An inverse homogenization problem. *Int. J. Solids. Struct.* **31**, 2313-2329 (1994). doi: 10.1016/0020-7683(94)90154-6

14. O. Sigmund, Tailoring materials with prescribed elastic properties. *Mech. Mater.* **20**, 351-368 (1995). doi: 10.1016/0167-6636(94)00069-7

15. P. Vogiatzis, S. Chen, X Wang, T Li, L Wang, Topology optimization of multi-material negative Poisson's ratio metamaterials using a reconciled level set method. *Comput. Aided. Des.* **83**, 15-32 (2017). doi: 10.1016/j.cad.2016.09.009

16. A. Clausen, F. Wang, J. S. Jensen, O. Sigmund, J. A. Lewis, Topology Optimized Architectures with Programmable Poisson's Ratio over Large Deformations. *Adv. Mater.* **27**, 5523-5527 (2015). doi: 10.1002/adma.201502485

17. R. Lakes, Foam structures with a negative Poisson's ratio. *Science* **235,** 1038-1041 (1987). doi: 10.1126/science.235.4792.1038

18. D. Prall, R. S. Lakes, Properties of a chiral honeycomb with a poisson's ratio of -1. *Int. J. Mech. Sci* **39** 305-307 (1997). doi: 10.1016/S0020-7403(96)00025-2

19. C. S. Ha, M. E. Plesha, R. S. Lakes, Chiral three-dimensional isotropic lattices with negative Poisson's ratio. *Phys. Status Solidi B* **253** 1243-1251 (2016). doi: 10.1002/pssb.201600055

20. S. Babaee *et al.* 3D Soft Metamaterials with Negative Poisson's Ratio. *Adv. Mater.* **25**, 5044-5049 (2013). doi: 10.1002/adma.201301986

21. T. Bückmann *et al.*, On three-dimensional dilational elastic metamaterials. *New J. Phys.* **16** 033032 (2014). doi: 10.1088/1367-2630/16/3/033032

22. R. Gatt *et al.*, Hierarchical Auxetic Mechanical Metamaterials. *Sci. Rep.* **5**, article 8395 (2015). doi: 10.1038/srep08395

23. E. Andreassen, B. S. Lazarov, O. Sigmund, Design of manufacturable 3D extremal elastic microstructure. *Mech. Mater.* **69** 1-10 (2014). doi: 10.1016/j.mechmat.2013.09.018

24. K. K. Saxena, R Das, E. P. Calius, Three decades of auxetics research - materials with negative Poisson's ratio: a review. *Adv. Eng. Mater.* **18**, 1847-1870 (2016). doi: 10.1002/adem.201600053

25. B. Zhu, M. Skouras, D. Chen, W. Matusik, Two-Scale Topology Optimization with Microstructures, *ACM Trans. Graph.*, in press (available at http://people.csail.mit.edu/desaic/pdf/tto.pdf)

26. J. B. Tenenbaum, V. de Silva, J. C. Langford, A global geometric framework for nonlinear dimensionality reduction, *Science.* **290**, 2319-2323 (2000). doi: 10.1126/science.290.5500.2319

27. G. McLachlan, T. Krishnan. *The EM algorithm and extensions*. Vol. 382. John Wiley & Sons, 2007.

28. T. Lee, R. L. Kashyap, C Chu, Building skeleton models via 3-D medial surface axis thinning algorithms. *Graph. Model. Im. Proc.* **56**, 462-478 (1994). doi: 10.1006/cgip.1994.1042

29. The database of microstructures reported in the paper are available at the following link: https://www.dropbox.com/sh/oejrntg5murl1bv/AACZv-JxCoRmH5zaekRCz3l7a?dl=0.

30. J. Guedes, N. Kikuchi, Preprocessing and postprocessing for materials based on the homogenization method with adaptive finite element methods. *Comput. Methods Appl. Mech. Eng.* **83,** 143-198 (2003). doi: 10.1016/0045-7825(90)90148-F

31. L. Xia, P. Breitkopt, Design of materials using topology optimization and energy-based homogenization approach in Matlab. *Struct. Multidisc. Optim.* **52**, 1229-1241 (2015). doi: 10.1007/s00158-015-1294-0

32. O. Sigmund, Morphology-based black and white filters for topology optimization. *Struct. Multidisc. Optim.* **4**, 401-424 (2007). doi: 10.1007/s00158-006-0087-x

33. J. H. Roh, C. B. Giller, P. H. Mott, C. M. Roland, Failure of classical elasticity in auxetic foams. *AIP Adv.* **3**, 042126 (2013). doi: 10.1063/1.4802925

34. R. W. Ogden, Non-Linear Elasic Deformations (Dover, New York, 1997).

35. Materials and methods are available as supplementary materials.

36. K. Bertoldi, P. M. Reis, S. Willshaw, T Mullin, Negative Poisson's Ratio Behavior Induced by an Elastic Instability. *Adv. Mater.* **3**, 361-366 (2010). doi: 10.1002/adma.200901956

37. A. Alderson *et al.*, Elastic constants of 3-, 4- and 6-connected chiral and anti-chiral honeycombs subject to uniaxial in-plane loading. *Compos. Sci. Technol.* **70**, 1042–1048 (2010). doi: 10.1016/j.compscitech.2009.07.009

38. J. Wu, C. Dick, R. Westermann, A system for high-resolution topology optimization. *IEEE Trans. Vis. Comput. Graphics*, **22** 1195-1208 (2016). doi: 10.1109/TVCG.2015.2502588

39. K Svanberg, The method of moving asymptotes-a new method for structural optimization. *Int. J. Numer. Methods Eng.* **24,** 359-373 (1987).
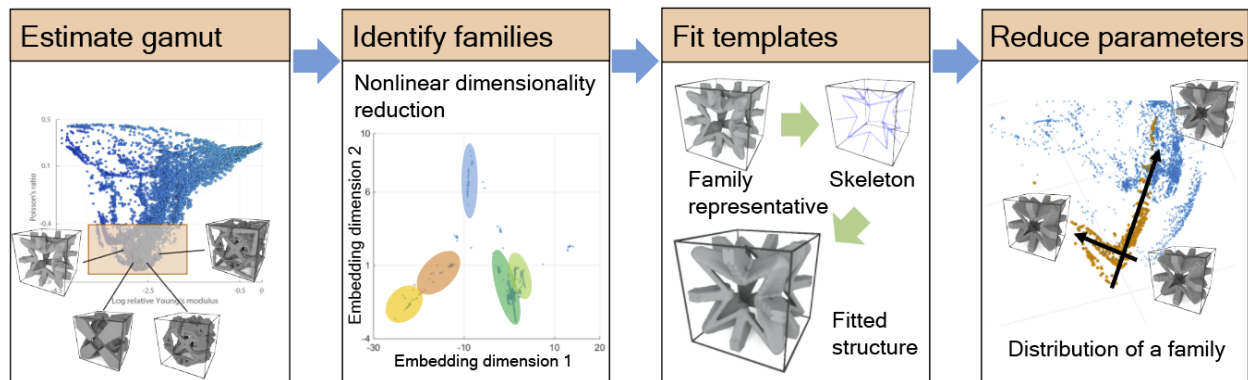
Fig. 1. A computational process for discovery of extremal microstructure families. Given a set of physical properties and design constraints, we estimate the material property gamut using stochastic sampling and topology optimization. Structures near the gamut boundary are grouped into families using nonlinear dimensionality reduction. A representative from each family is fitted with a template represented as a skeleton. Beams are placed on the skeleton edges with optimized parameters to fit the original structure. Structure variations with the same topology can be generated by varying the beam parameters. Finally, reduced template parameters are computed to reveal domain-specific design principles.
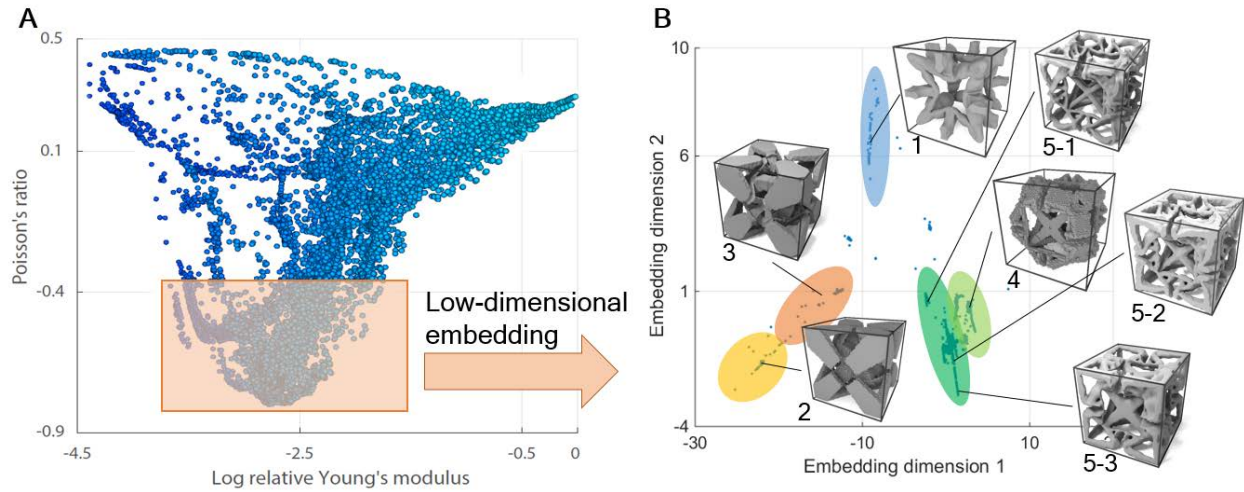
Fig. 2. Five microstructure families identified by nonlinear dimensionality reduction (NLDR). Structures with similar properties in the gamut (A) are selected to study their commonalities. We focused on structures with negative Poisson's ratio (auxetics) since they exhibit more complex structures. Auxetic families are identified in the embedding space numbered from 1 to 5 (B). Families with similar topologies are located closer in the embedding space. Three example structures from family 5 show underlying connection between seemingly distinct structures through gradual morphing of shape.
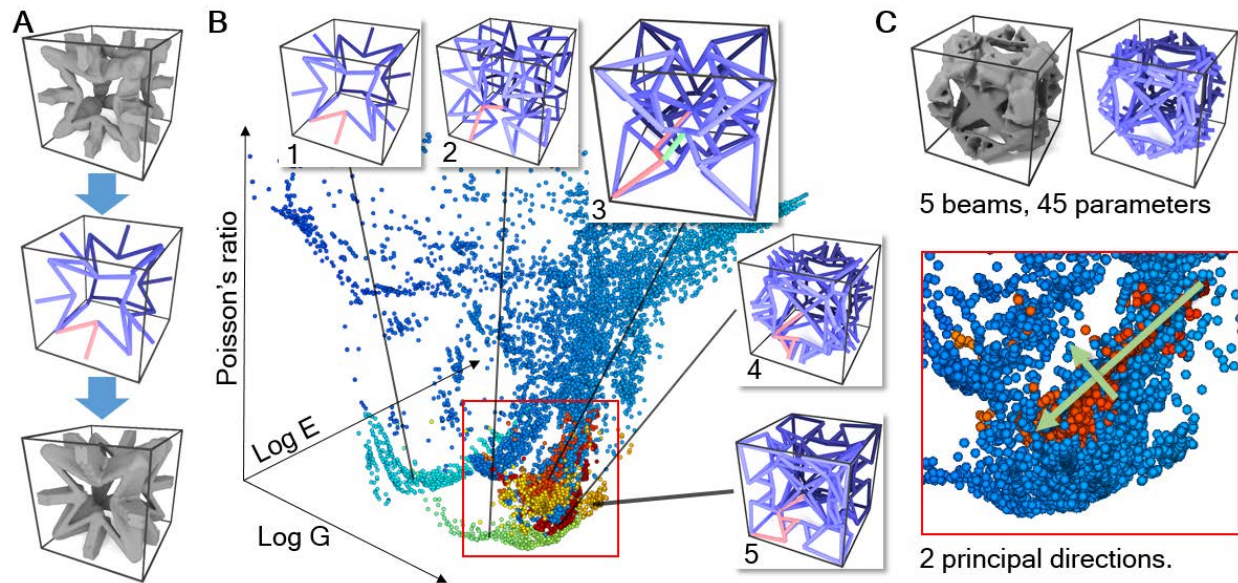
Fig. 3. Sampled coverage of microstructure templates in the gamut. (A) Extracting a skeleton (middle) from a representative structure (top). The skeleton represents the topology of the structure. A beam network is derived from the skeleton by placing a cuboid on each edge of the skeleton. Since we enforce cubic symmetry, the beams in a single tetrahedron determine the entire beam network. A template can generate a new structure (bottom) that approximates the original structure. (B) Coverage of each template in the material property space. (C) Reducing template parameter dimensions with principal component regression. The first two reduced parameters approximately correspond to varying the Young's modulus and Poisson's ratio of a structure.
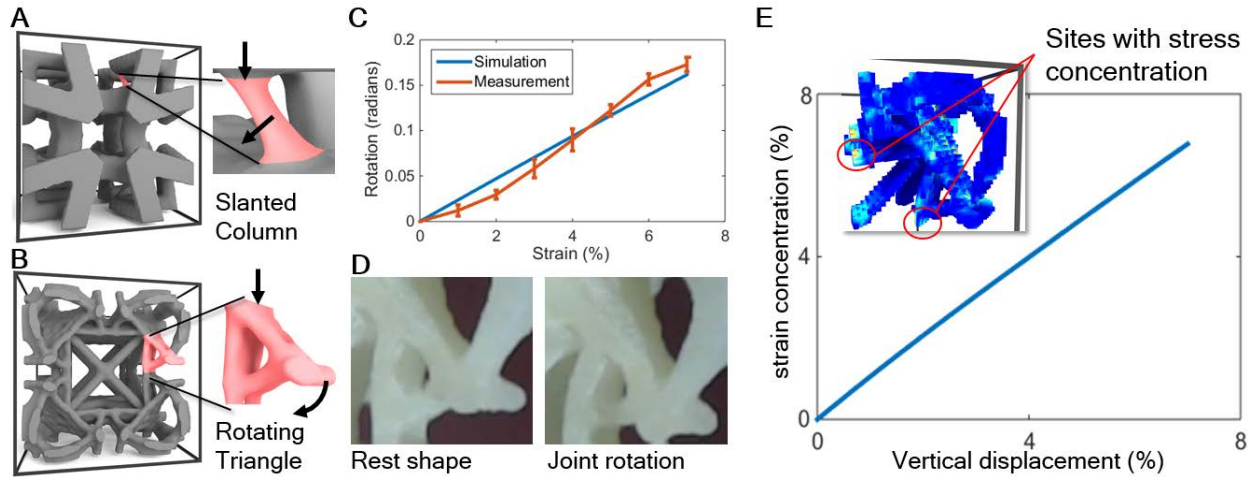
Fig. 4. Discovered auxetic mechanisms. Two mechanisms capable of producing auxetic behavior are discovered from our microstructure families. The slanted column (**A**) transforms vertical stress into horizontal displacement. The rotating triangle mechanism (**B**) pulls the outer tip of the joint towards the center of the structure, reducing the macroscopic volume. (**C**) The relationship between vertical strain and rotation of the triangle joint. The rotation is observed in printed samples under vertical load (**D**). Stress is concentrated at the lower end of the triangle joint (**E**).

Materials and Methods

Figures S1-S7

Tables S1

Movies S1-S3